Acta Scientiarum
http://periodicos.uem.br/ojs
ISSN on-line: 1807-8664
Doi: 10.4025/actascitechnol.v44i1.57848

Fault current and fault voltage analysis of power transmission systems with high penetration of inverter-based wind generators

Moisés Junior Batista Borges Davi[1*], David Calhau Jorge[1] and Felipe Vigolvino Lopes[2]

[1]Programa de Mestrado Profissional em Inovação Tecnológica, Universidade Federal do Triângulo Mineiro, Avenida Doutor Randolfo Borges Júnior, 1400, 38064-200, Uberaba, Minas Gerais, Brazil. [2]Universidade Federal da Paraíba, João Pessoa, Paraíba, Brazil. *Author for correspondence. E-mail: moises.davi.eng@hotmail.com

ABSTRACT. This paper highlights the evolution of wind power sources in the modern energy scenario, emphasizing the impacts of inverter-based generators, namely Full-Converter and DFIG (Doubly-Fed Induction Generator), on fault currents and fault voltages in transmission systems. The studies were carried out through computer simulations, with an EMTP (Electromagnetic Transients Program) type software. A power system with high penetration of such renewable generations was modeled and several contingency scenarios were simulated in a transmission line that performs the connection of the wind power plant to the grid. The scenarios included the variation of parameters such as fault type, inception instant angles, resistance, and distance, to explore the main differences between the contributions to the fault of a wind power plant and conventional generation. Among the atypical analyzed characteristics, the following can be highlighted: the absence of the DC (Direct Current) component for Full-Converter generation, independent of fault inception instant angle and distance variation; low levels of the fault contributions at the wind power plant terminal; low levels of voltages at the wind power plant terminal, evidencing the high SIR (Source Impedance Ratio) characteristic of these generations; atypical relations between the fault resistance and measured currents; and others. The obtained results show the importance of further studies on the impacts of inverter-based generations on fault currents and voltages, allowing developments that are able to improve control and protection systems for grids with high penetration of this wind generation topologies.

Keywords: wind turbine; renewable energy; DFIG; full-converter; protection system.

Received on February 17, 2021.
Accepted on October 25, 2021.

Introduction

Wind energy is becoming increasingly important in the energy scenario of modern electrical systems. In the last 20 years, the total generation capacity installed worldwide has increased from 24 GW in 2001 to 743 GW in 2020 (Lee & Zhao, 2021). As described in (Chen, Guerrero, & Blaabjerg, 2009), there are several topologies of wind power generation units. Among those arising concern from researchers in the electrical sector, the DFIG (Type III) and Full-Converter (Type IV), which use converters to interface generation units with the primary grid, stand out.

Historically, these generations account for a relatively low percentage of the power system generation capacity and, therefore, they used to be quickly disconnected under grid disturbance conditions. However, the disconnection of these generations has become critical for system stability, due to their increasing penetration. Consequently, requirements called Fault Ride-Through have been adopted by several countries, so that wind generations have the ability to stay connected to the system, even under disturbance conditions (Piya, Ebrahimi, Karimi-Ghartemani, & Khajehoddin, 2018).

With such new requirements and the increasing penetration of DFIG and Full-Converter generation topologies into existing grids, clarifications on the impacts of these generations, mainly in the operation of protective relays, have attracted the interest of researchers. Considering that the largest wind power plants are connected to transmission and sub-transmission systems, several studies on the impact of wind generations on distance protection functions have been conducted (Hooshyar, Azzouz, & El-Saadany, 2015; Wu, Lin, Lee, Hsieh, & Lin, 2016; Fang, Jia, Yang, Li, & Bi, 2019; Banaiemoqadam, Hooshyar, & Azzouz, 2020). A major focus has also been given to the operation of the directional (Jia, Yang, Fang, Bi, & Sumner, 2019; Haddadi, Kocar, & Farantatos, 2019) and phase-selection functions (Hooshyar, El-Saadany, & Sanaye-Pasand, 2016; Azzouz, Hooshyar, & El-Saadany, 2018).

It can be seen that most works in this area focus on the impacts of inverter-based wind power generations (Full-Converter and DFIG) on the operation of protection functions, i.e., on final applications that depend on how these generations influence on the measured current and voltage signals. However, for a comprehensive understanding of these impacts, analyses must be performed on the measured current and voltage signals, before they are processed by each protection function. In this sense, the literature still lacks a paper that encompasses the detailed analysis of the current and voltage waveforms, evaluating the impact of DFIG and Full-Converter generators, simultaneously, and presenting the obtained waveforms for different fault parameters such as resistances, inception instant angles, and fault locations.

Motivated by the abovementioned context, this work provides detailed evaluations of fault currents and fault voltages waveforms, considering systems with high penetration of DFIG and Full-Converter generation topologies. Symmetrical and asymmetrical fault scenarios are simulated, varying the fault resistances, locations, and inception instant angles. By doing so, the main differences between the fault contributions of inverter-based wind power plants and conventional generations are addressed in detail.

Material and methods

Fundamentals of inverter-based wind power generation

The first wind power generation systems were composed of squirrel cage rotor induction generators, directly connected to the grid, and turbines with a fixed speed, that is, the turbines were designed to obtain maximum efficiency with a certain wind speed that, when varying, resulted in mechanical stresses and power quality problems (Chen, Guerrero, & Blaabjerg, 2009).

From the development of wind turbines with higher power output, the concept of regulation in frequency, voltage, and generated power became important. It requires the use of power electronics devices, to act as an interface between the turbine and the grid. Therefore, wind generation started to operate as a controlled source of active power to the grid (Blaabjerg, Liserre, & Ma, 2012). The operating characteristics of the main inverter-based generation topologies will be explored.

DFIG generation topology (type III)

DFIG generators operate with the same principles as conventional induction generators. However, in DFIG topology power electronics circuits are used to regulate and optimize the available mechanical energy provided from the wind. In this topology, the machine's stator winding is powered directly by the grid voltage, normally with a voltage level below 1 kV and a system frequency of 50 or 60 Hz. The rotor winding is powered by an AC-DC-AC converter, and as only part of the active power flows through the rotor circuit, the converter power is usually about 20 to 30% of the machine's nominal power (Chen, Guerrero, & Blaabjerg, 2009).

The rotor-side converter is connected to the grid-side converter using a DC link. Assuming that the grid-side converter keeps the DC link voltage fixed, the rotor-side converter is responsible for injecting currents with different frequencies inside the rotor, to obtain decoupled control of the generated active and reactive power. When the wind turbine operates below synchronous speed, the applied excitation creates an apparent field with rotation in the same direction as the mechanical rotor. The magnetic field seen from the stator is the resulting rotation speed equals to the sum of the mechanical rotor speed and the apparent field caused by the rotor excitation. Similarly, when the wind turbine operates above synchronous speed, a negative sequence excitation is applied to the rotor, causing the apparent field to have a rotation opposite to the its physical direction. Thus, for both operation modes, the frequency and phase sequence of the rotor excitation are such that the net rotation of the magnetic field is at synchronous speed.

The couple sequence control is typically employed in this topology. It allows dissociating the active and reactive power control, operating with the DQ reference, namely Park transform. The DQ reference can decompose currents in active and reactive power components, those components can be adjusted to previous values using PI controllers (proportional-integral). It's possible to compare the power values measured at the terminal of the generation system to the set values, which depend on the wind speed. The controllers will define the D and Q axis currents required to generate the expected power values. Once the necessary DQ currents have been set, they are converted back to phase reference (ABC), and using a pulse generation control to the converter's IGBTs the currents are injected into the machine's rotor. On the grid side, the control is responsible to maintain the voltage on the DC link constant and balancing the power injected into it and the power supplied to the grid (Singh & Santoso, 2011).

Some of the advantages of DFIG topology are: independent active and reactive power controls, wide speed range on the generator shaft of up to 30% below and above the rated speed with minimum losses, and maximized wind energy extraction. Dynamic models to represent the DFIG topology and more details related to the controllers used for this generation type can be found in (Ekanayake, Holdsworth, Wu, & Jenkins, 2003).

Full-converter generation topology (type IV)

Full-Converter topology generating units typically consist of a synchronous generator, a turbine, and an AC-DC-AC converter (Conroy & Watson, 2007).

The AC-DC-AC converter is responsible for decoupling the generator from the grid, improving the response to failures, allowing the turbine to operate at a wide speed range, and optimizing the extraction of wind energy. It should be noted that the gearbox in this topology may not be necessary for some wind turbines, depending on the design and number of generator poles (Conroy & Watson, 2007).

It is worth mentioning that the Full-Converter topology is more expensive since, unlike the DFIG topology where the converter handles 30 to 40% of the generator output power, in this case, the converter must handle 100% of the generator output power. On the other hand, it is possible with this topology to operate with a speed variation of about 2.5 times the generator's nominal speed. The generator is uncoupled from the grid, so the voltage and frequency variations in the grid are not directly reflected in the generator, which differentiates this topology from others (Conroy & Watson, 2007).

The AC-DC converter typically consists of a diode rectifier bridge and a Boost topology DC-DC converter for voltage control on the DC link (Chen, Guerrero, & Blaabjerg, 2009). The Boost converter controller is based on a comparison between the output of a PI control and a triangular waveform for pulse generation to the converter's IGBTs. The topologies that employ 6-pulse bridges with IGBTs can also be found for voltage control in the DC link (Singh & Santoso, 2011).

Finally, the DC to AC conversion is performed by a current-controlled voltage source type inverter, capable of decoupling the regulation of the active and reactive powers generated. Such control is based on the DQ reference variables, as seen for the DFIG topology, allowing currents to be decomposed into an active power component and a reactive power component. Active and reactive power reference signals are compared with measured values and used to trigger independent PI controllers. The outputs of these controllers are used to obtain the reference currents, which are finally transformed back into the phase reference, and dictate the behavior of the pulse generation systems for the inverter's IGBTs. Models for the representation of the Full-Converter topology and more details related to the operation of the controls used for this generation type can be found in (Conroy & Watson, 2007).

Proposed test system for the study

The studied power system parameters are shown in Table 1 and illustrated in Figure 1, including a wind power plant composed of 96 wind turbines. The modeling was done through the software MATLAB-Simulink. The proposed system includes a Thevenin equivalent, with a voltage level of 500 kV and 60 Hz frequency. The connection of the wind farm to the grid is made by a 239 km transmission line (TL), represented in this case by distributed parameters and the Bergeron model. Power transformers responsible for raising the voltage from generation levels to sub-transmission levels (delta-star connection) and finally to the transmission levels (star-star connection) were also represented.

Verifying the main inverter-based wind generation topologies, the system was modeled considering both DFIG and Full-Converter type generators. The active and reactive power supplied by the generating units are controlled at 220 MW and 0 VAr, respectively.

For modeling the Full-Converter generators, synchronous machines were used and all controls were set as described in (Aziz, MTO, & Stojcevski, 2016). The DC link consists of a 0.09 Farad capacitor with a nominal voltage of 1100 The coupling choke circuit has a resistance of 0.003 p.u. and inductance of 0.15 p.u. at the machine base, and the RC output filter has a power of 120 kVAr. The nominal data for the synchronous generators are: S_n = 1.67 MVA, V_n = 730 V, R_s = 0.006 p.u., X_l = 0.18 p.u., X_d = 1.305 p.u., X'_d = 0.296 p.u., X''_d = 0.252 p.u., X_q = 0.474 p.u., X''_q = 0.243 p.u., T'_{do} = 4.49 s, T''_{do} = 0.0681 s e T''_q = 0.0513 s.

Table 1. Proposed system parameters.

Parameters	Value
Equivalent System	500 kV - 10 GVA - X/R = 10
Transformer D-Yn 34.5 – 0.575 kV	1.75 MVA - Z = 6%
Transformer Yn-D 138 – 34.5 kV	90 MVA - Z = 10%
Feeder (18 km)	R = 0.191 ohm km^{-1} L = 1.192 mH km^{-1}
Transformer Yn-Yn 500 – 138 kV	360 MVA - Z = 10%
Transmission Line (239 km)	R+/0 = 0.0191/0.2044 ohm km^{-1} L+/0 = 0.818/2.17 mH km^{-1} C+/0 = 0.0142/0.009 µF km^{-1}

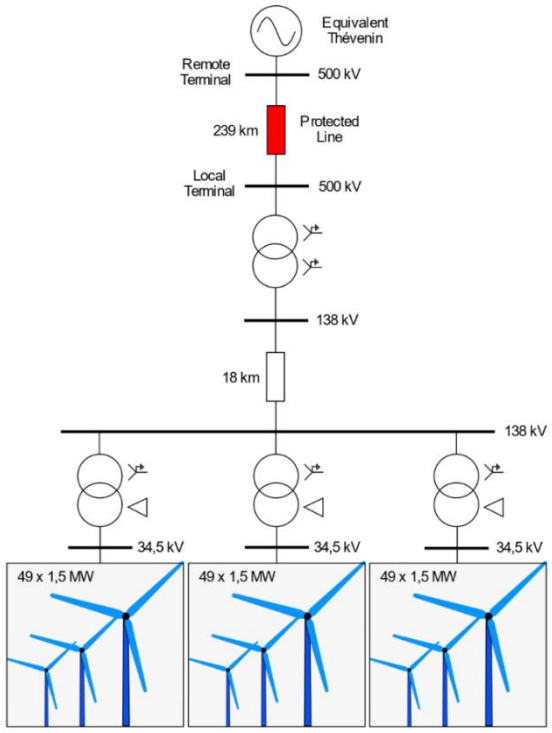

Figure 1. Single-line diagram of the proposed test system.

To model the DFIG unit, all controls were adjusted as described in (Ekanayake, Holdsworth, Wu, & Jenkins, 2003). The DC link consists of a 0.01 Farad capacitor with a nominal voltage of 1150 The coupling choke circuit has a resistance of 0.003 p.u. and inductance of 0.3 p.u. at the machine base, and the RC output filter has a power of 120 kVAr. The crowbar circuit was designed to operate when the measured rotor current exceeds 4 p.u. or when the DC link voltage exceeds 1.2 p.u., and is kept active for a total time of 60 millis after its operation. The nominal data for the induction generators are: S_n = 1.67 MVA, V_n = 575 V, R_s = 0.023 p.u., R_r = 0.016 p.u., X_m = 2.9 p.u., X_s = 0.18 p.u. e X_r = 0.16 p.u.

To analyze the contribution of the wind farm through faults in the electrical system, faults in the 239 km TL were simulated, varying the resistance (0 Ω, 20 Ω, 50 Ω, 100 Ω, and 200 Ω), the inception angle (0°, 45° and 90° with sine angle reference), the distance from the remote terminal (0, 20, 40, 60, 80, and 100%) and the type (Single-phase-to-ground - PG, and Three-phase - PPP, with P being the faulted phase) of fault, resulting in a total of 180 simulated scenarios. In all scenarios, the fault starts at 1.1 s.

Result and discussion

Considering the obtained results, analyses on the behavior of electrical quantities were carried out, evaluating the influence of 1) fault inception instant angle, 2) fault resistance, and 3) fault location variation on the fault voltages and currents.

Influence of the fault inception instant angle variation on the fault voltages and currents

The variation of the fault inception instant angle results in different characteristics of the transients in the first moments after the short circuit. Among the characteristics influenced by this variation, the following can be highlighted: modification of the content of high-frequency components in the monitored signals and amplitude of the exponential decay DC component (Anderson, 1999). Such characteristics can significantly modify the performance of some protection functions, whether they are based on high-frequency components such as traveling waves (Chen, Malik, Yin, Chen, & Zhang, 2003), for example, or even based on the polarity and amplitude of the DC component of fault current, such as phase comparison protection with the use of instantaneous magnitudes.

In this context, simulations of three-phase faults at 50% of the protected TL were carried out, taking into consideration three different values for the fault inception instant angle (0°, 45°, and 90°). Faults initiated at instant t = 1.1 s were considered. After this, the current in phase A was monitored at the local and remote terminals, taking into account the DFIG and Full-Converter generations. The results obtained are shown in Figure 2 to 5.

Regarding the currents measured at the remote terminal, for both considered generation topologies (DFIG and Full-Converter), Figure 2 shows the expected behavior for the current in phase A, with minimum peak values for the inception angle of 90°, intermediate values for 45° and maximum values for 0°. Such differences in peak values in initial cycles occur due to the DC component characteristic of RL type systems (resistances and inductances in series). It is possible to see that the peak value of just over 15 A (90° angle) is increased to levels of approximately 30 A, i.e. the DC component of the circuit practically doubles the peak value obtained after the fault.

At the local terminal, it is observed by Figure 3 and 4, that the current levels of the fault period are significantly lower if compared to the levels obtained at the remote terminal. This condition is justified both by the inverter-based generation topologies, which include limiting controls to protect the power electronics devices that are part of the topology and by the fact that the short circuit level at the local terminal is considerably lower, characterizing it as a weak terminal.

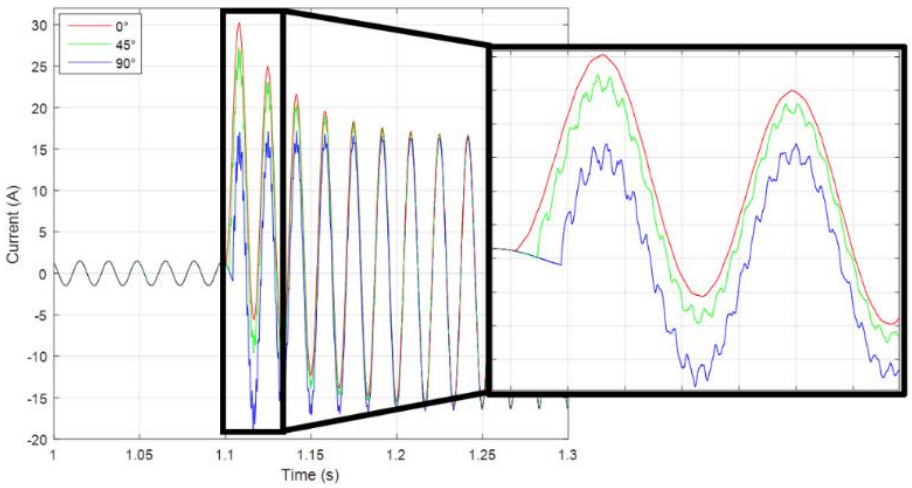

Figure 2. Remote terminal currents (Conventional Generation).

It is also observed that for the DFIG generation, the incidence angle had an influence on the peak values for the initial fault cycles, similarly to what occurred at the remote terminal, even at lower levels, while for the Full-Converter generation topology, no significant differences were observed in the fault currents, except for the high-frequency components, obtained for different incidence angles. It should also be noted that the contribution of the DFIG generation was higher than that of the Full-Converter generation, which is similar to the one highlighted in the literature that for Full-Converter generations the contributions are limited between 1 and 1.2 times the nominal current, while for DFIG topologies these values may be higher since there is a direct connection of the machine stator to the grid (Institute of Electrical and Electronics Engineers [IEEE] & North American Electric Reliability Corporation [NERC], 2018).

It can also be noted that the high-frequency components in the monitored signals presented similarities for all types of generation, with such components being more representative for faults with an inception

instant angle of 90°, with intermediate representation for faults with an angle of 45° and being suppressed in scenarios with an angle of 0°.

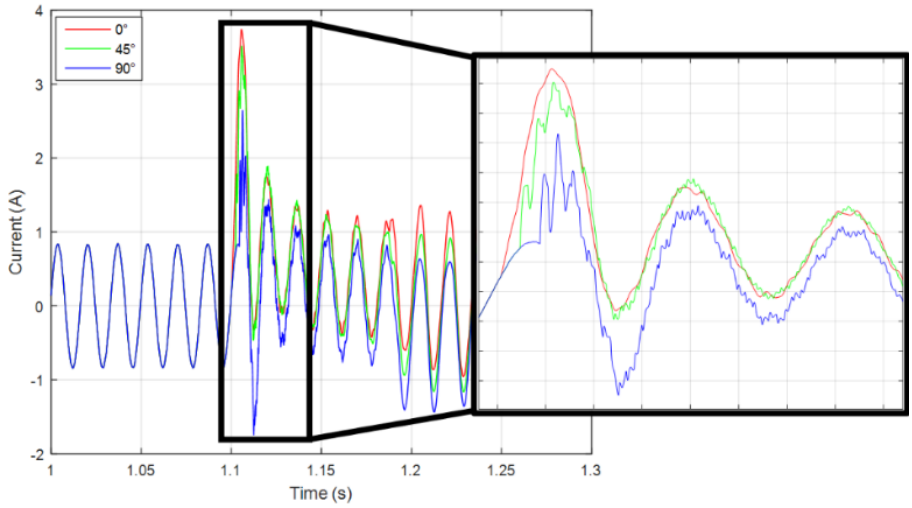

Figure 3. Local terminal currents (DFIG Generation).

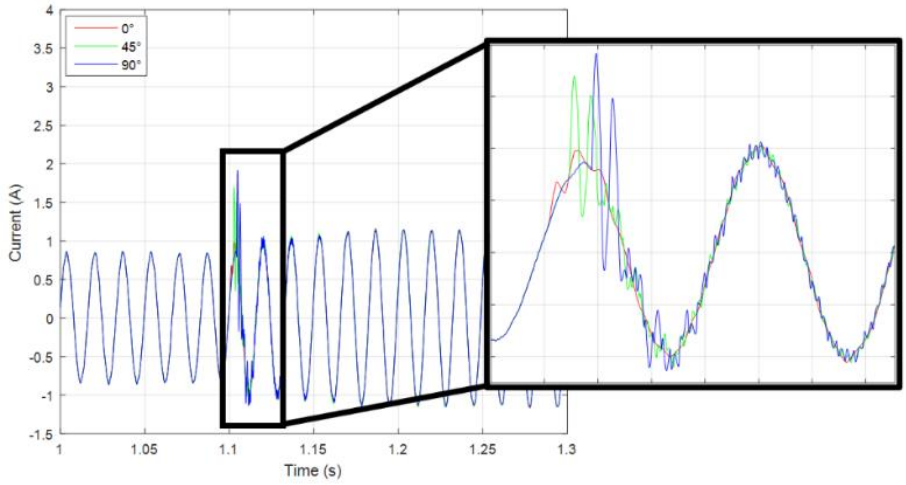

Figure 4. Local terminal currents (Full-Converter Generation).

Influence of the fault resistance variation on the fault voltages and currents

As well as the inception instant angle, the fault resistance is a determining factor in the characterization of the contribution levels and oscillographs obtained during short-circuit occurrences. For faults with the involvement of low resistances, the contribution levels for conventional generations are generally quite high. Such levels tend to be reduced as the fault resistance increases, and may cause undue operations or no operations of certain protection functions such as distance (21), which have their decision based on monitoring the impedance seen by the terminal, or also overcurrent functions (67N, 67Q or 50N/51N, for example) which are sensitized by current thresholds that may not be reached due to the high fault resistance.

In order to verify this characteristic, A-G fault scenarios were simulated at 50% of TL, with an inception instant angle of 90°, varying the fault resistance between the values of 0 Ω, 20 Ω, 50 Ω, 100 Ω, and 200 Ω. Faults initiated at instant t = 1.1 s were considered and Figure 5 to 7 illustrate the monitored voltages and currents in phase A of both TL terminals.

Regarding the voltages and currents measured at the remote terminal, for both considered generation topologies (DFIG and Full-Converter), Figure 5 shows the expected behavior since as the fault resistance increases, the fault current levels are considerably reduced while the voltage levels tend to reach nominal values. Significant variations have been observed both in current peaks (between values of 12.5 A - 0 Ω up to values of 3 A - 200 Ω) and in the voltage peaks (between values of 62 V - 0 Ω up to values of 91 V - 200 Ω).

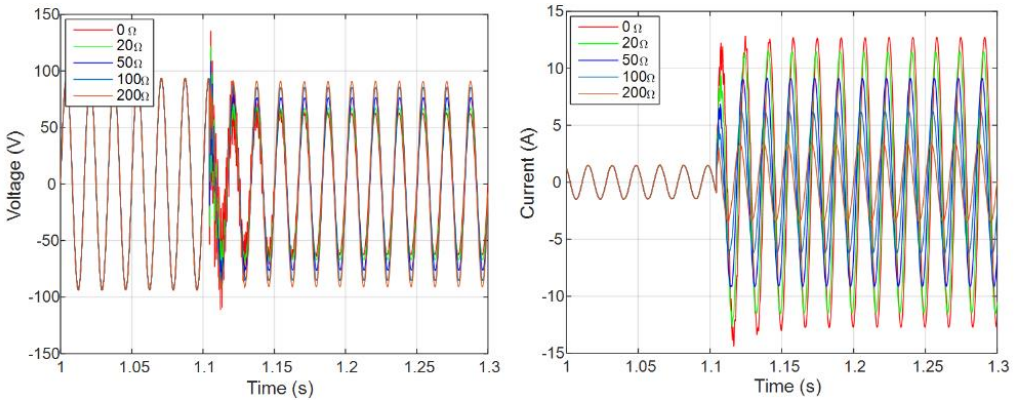

Figure 5. Remote terminal voltages and currents (Conventional Generation).

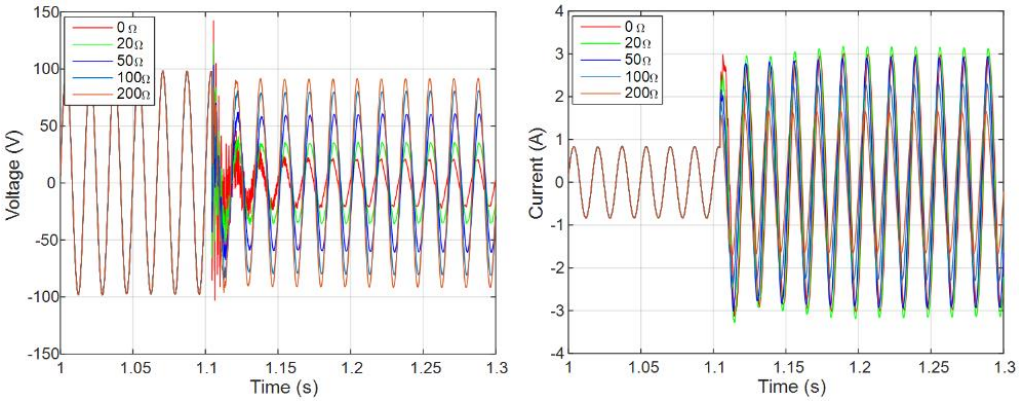

Figure 6. Local terminal voltages and currents (DFIG Generation).

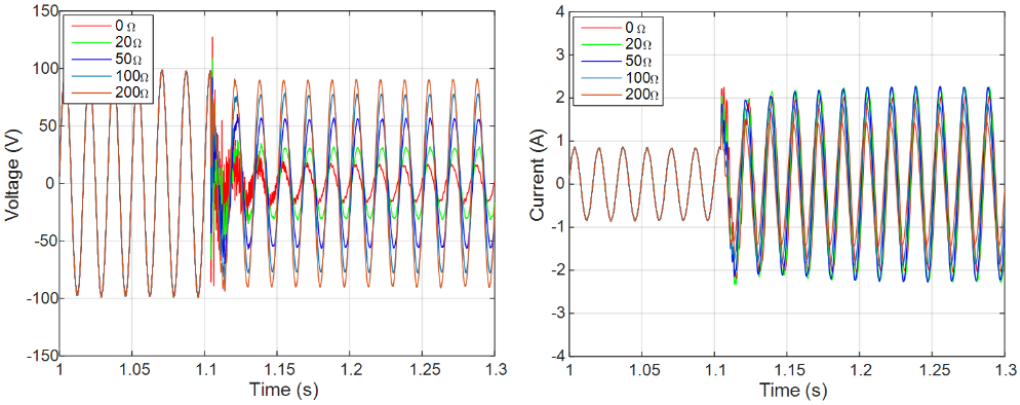

Figure 7. Local terminal voltages and currents (Full-Converter Generation).

For the voltages measured at the local terminal, more significant variations can be observed than those observed at the remote terminal (between values of 17 V - 0 Ω up to values of 91 V - 200 Ω), and the levels tend to reach nominal values as the fault resistance increases. Regarding the currents measured at the local terminal, shown in Figure 6 and 7, a less significant influence of the fault resistance can be observed in the current peaks obtained (smaller variations if compared to the variations obtained at the remote terminal), since the operation characteristics of the DFIG and Full-Converter topologies themselves already result in low contribution levels of these generations to faults. It is also possible to verify that the current levels obtained for the fault with no resistances were slightly lower than the values obtained for resistances of 20 Ω (for DFIG and Full-Converter generations) and 50 Ω (for Full-Converter generation), which evidences an atypical behavior of the inverter-based generations, since for conventional generations it was found that the increase in the fault resistance reflected in the decrease of the faulted phase current.

Aiming to clarify the slightly higher levels for the phase A currents in some fault scenarios involving resistances, Figure 8 illustrates the phase currents as well as the magnitude and phase angle of sequence

currents measured at the local terminal for Full-Converter generations. An A-G fault at 50% of TL is considered, assuming an inception instant angle of 90° and with 0 Ω and 50 Ω fault resistances.

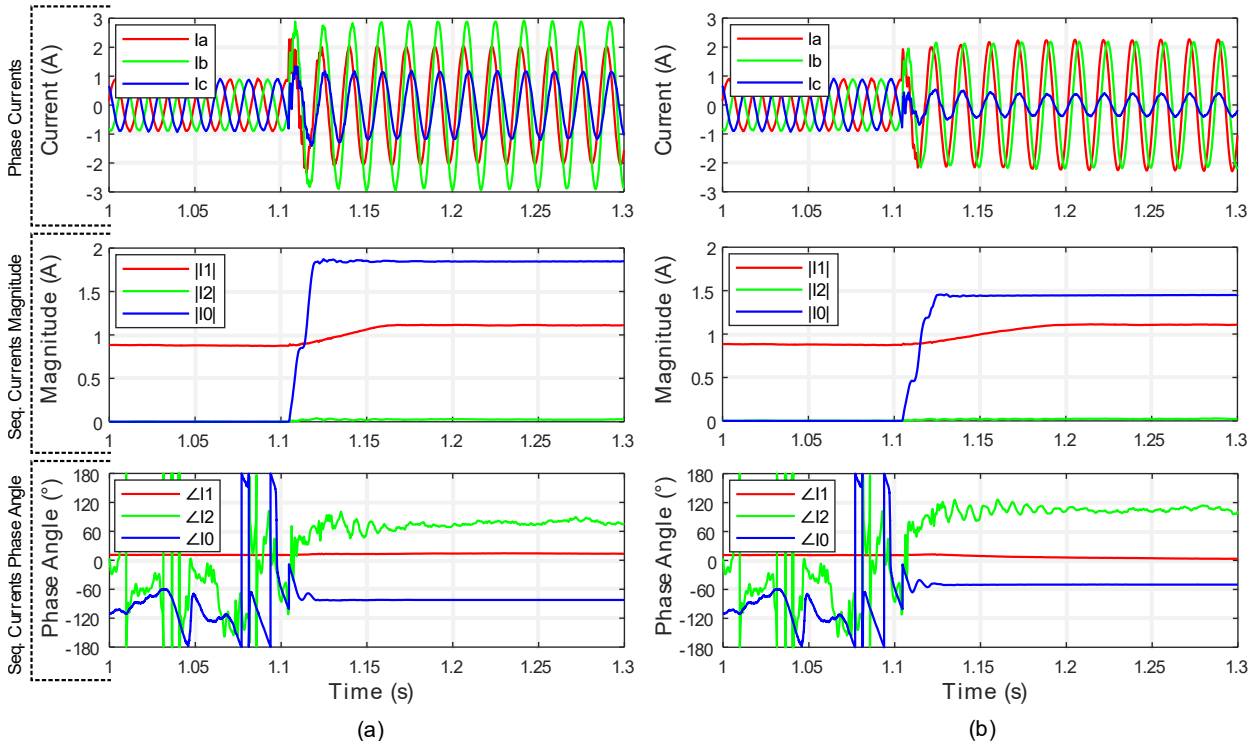

Figure 8. Local terminal phase and sequence currents considering an A-G fault with resistances of (a) 0 Ω and (b) 50 Ω (Full-Converter Generation).

Regarding the fault scenario without fault resistance, it is first observed that the phase A current does not present magnitudes higher than those of the other phases, which would be expected for A-G faults in systems with conventional generations. Furthermore, it is observed that, after the fault inception, the currents are almost in phase, evidencing the dominance of the zero-sequence component in these currents, since the positive sequence component is limited by the converter's controls. The suppression of the negative sequence currents can be also noticed, being a particular characteristic of the Coupled Sequence Control employed in this work for the converters, which is typically employed in Full-Converter generators (Kauffmann et al., 2019).

Analyzing the scenario with a 50 Ω fault resistance, it is observed that the magnitude and phase angle of positive sequence current are practically the same as in the scenario without fault resistance. However, the fault resistance significantly changes the magnitude and phase angle of zero sequence current. As a consequence of these changes, magnitudes of the phases B and C currents decrease, while the magnitude of the phase A current is maintained at values slightly higher than those obtained for the solid fault scenario.

Therefore, the slightly higher levels for the phase A currents in fault scenarios involving resistances, if compared with the solid fault cases, is justified by the operation of the converter's control, which results in quite atypical characteristics for the measured fault contributions. The main characteristics that stand out are the limitation of the positive sequence contribution levels and the suppression of the negative sequence current, which make the fault contributions from Full-Converter generators quite unpredictable.

For the DFIG topology, such occurrences are also justified by the converter's control action, with the difference that the suppression of negative sequence currents is not a characteristic of the controls usually employed in this topology (Morren & Haan, 2007). However, it is worth mentioning that there are strategies that also allow the suppression of negative sequence currents for the DFIG topology (Chen, Zhang, & Fan, 2020), which were not taken into account in this paper.

Influence of the fault location variation on the fault voltages and currents

The fault location variation will also have a significant influence on the currents and voltages measured at the TL terminals. For conventional generations, it is expected that as the fault approaches the TL terminal, the higher the currents and the lower the voltages measured at that terminal in the phases under fault will be.

For the performed analyses, three-phase faults with an inception instant angle of 90° and without fault resistance were simulated at several points of the TL (0, 20, 40, 60, 80, and 100%, being 0% at the remote terminal and 100% at the local terminal). Faults initiated at t = 1.1 s were considered. The positive sequence RMS values for voltages and currents were monitored and are illustrated in Figures 9, 10 and 11.

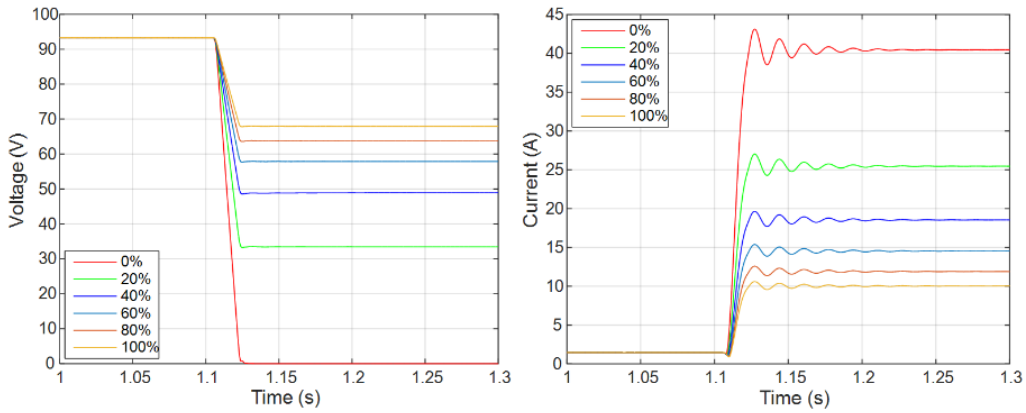

Figure 9. Remote terminal voltages and currents (Conventional Generation).

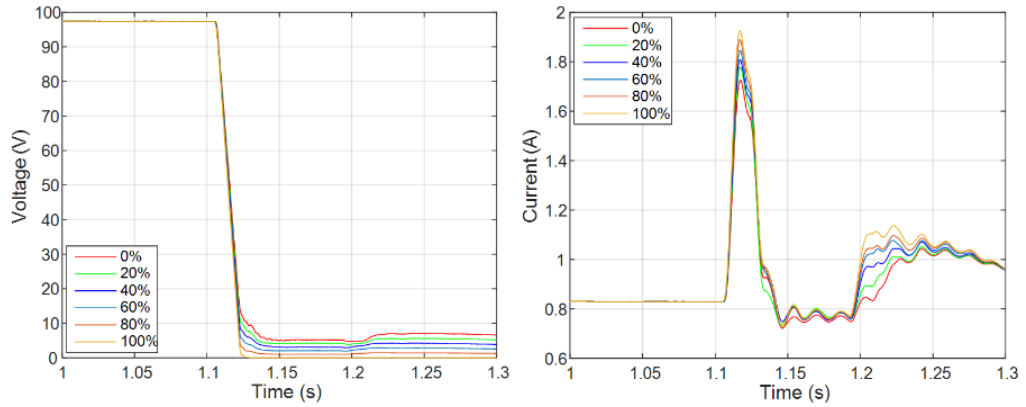

Figure 10. Local terminal voltages and currents (DFIG Generation).

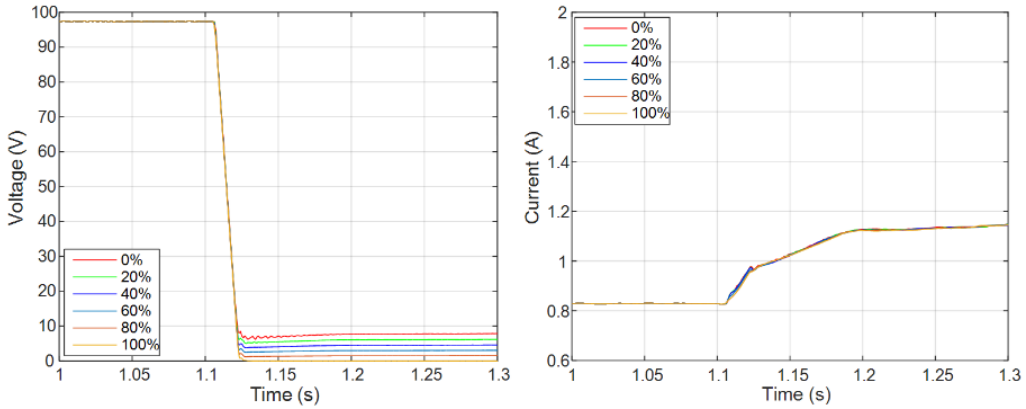

Figure 11. Local terminal voltages and currents (Full-Converter Generation).

Regarding voltages and currents measured at the remote terminal, for both considered generation topologies (DFIG and Full-Converter), the expected behavior is observed based on the literature, for a terminal with conventional generations. As the fault distances itself from the terminal, the voltages measured at that terminal tend to be higher and the currents lower, since the impedance between the measuring point and the fault point increases. Thus, for voltage, variations between values of 0 V (0% fault) and 70 V (100% fault) have been observed approximately, while for current, values between 40 A (0% fault) and 10 A (100% fault) have been reached.

For the local terminal, with regard to the measured voltages, it can be concluded that the simulated balanced fault in the scenarios evidenced the high SIR characteristic of the wind generation since the obtained

voltages had values lower than 10 V for all the simulated fault points, that is, the impedance from the measuring point to the source is significantly higher than the impedance from the measuring point to the fault point (TL impedance).

Regarding the currents, for the DFIG generation, it is observed that the magnitudes varied between 1.8 and 2.1 A in the initial cycles of fault. It is also important to point out the performance of the Crowbar protection circuit, typically observed in severe faults such as the one simulated in this scenario, after approximately 2 cycles from the beginning of the fault, which caused the reduction of the measured current levels to values close to those of a permanent regime. The Crowbar circuit acts to protect the generation system against high currents in the machine's rotor and/or high voltages in the converter's DC link (Hansen & Michalke, 2007).

For the Full-Converter generation, it is observed that all the measured fault currents were limited in approximately 1.13 A, highlighting the control limiting the characteristics of this topology.

Conclusion

This work highlighted the relevance of wind power sources in the energy scenario of modern electrical systems, emphasizing the main inverter-based generation topologies, Full-Converter and DFIG, and their impacts on fault currents and fault voltages of transmission systems.

The results of this paper show the importance of studies in the inverter-based generation area since several protection and control methodologies can be significantly affected by the atypical behavior of fault voltages and fault currents. In addition, the obtained results can also assist in the development or improvement of control and protection systems for grids with high penetration of this generation type.

References

Anderson), M. (1999). *Power system protection*. Piscataway, NJ: John Wiley & Sons Inc.

Aziz, A., MTO, A., & Stojcevski, A. (2016). Full convereter based wind turbine generator system generic modelling: Variations and appicability. *Sustainable Energy Technologies and Assessments,* 14, 46-62. DOI: https://doi.org/10.1016/j.seta.2015.12.001

Azzouz, M. A., Hooshyar, A., & El-Saadany, E. F. (2018). Resilience enhancement of microgrids with inverter-interfaced dgs by enabling faulty phase selection. *IEEE Transactions on Smart Grid, 9*(6), 6578-6589. DOI: https://doi.org/10.1109/TSG.2017.2716342

Banaiemoqadam, A., Hooshyar, A., & Azzouz, M. A. (2020). A control-based solution for distance protection of lines connected to converter-interfaced sources during asymmetrical faults. *IEEE Transactions on Power Delivery, 35*(3), 1455-1466. DOI: https://doi.org/10.1109/TPWRD.2019.2946757

Blaabjerg, F., Liserre, M., & Ma, K. (2012). Power electronics converters for wind turbine systems. *IEEE Transactions on Industry Applications, 48*(2), 708-719. DOI: https://doi.org/10.1109/TIA.2011.2181290

Chen, L., Zhang, B., & Fan, X. (2020). Asynmmetrical Fault Ride-Through Control Strategy for Rotor-Side Converter of DFIG. *IEEE Transactions on Energy Conversion,* 35(2), 1046-1053. DOI: 10.1109/TEC.2019.2963086.

Chen, W., Malik, O. P., Yin, X., Chen, D., & Zhang, Z. (2003). Study of wavelet-based ultra high speed directional transmission line protection. *IEEE Transactions on Power Delivery, 18*(4), 1134-1139. DOI: https://doi.org/10.1109/TPWRD.2003.817511

Chen, Z., Guerrero, J. M., & Blaabjerg, F. (2009). A Review of the State of the Art of Power Electronics for Wind Turbines. *IEEE Transactions on Power Electronics*, 24(8), 1859-1875. DOI: 10.1109/TPEL.2009.2017082.

Conroy, J. F., & Watson, R. (2007). Low-voltage ride-through of a full converter wind turbine with permanent magnet generator. *Renewable Power Generation, IET, 1*(3), 182-189. DOI: https://doi.org/10.1049/iet-rpg:20070033

Ekanayake, J. B., Holdsworth, L., Wu, X., & Jenkins, N. (2003). Dynamic modeling of doubly fed induction generator wind turbines. *IEEE Transactions on Power Systems, 18*(2), 803-809. DOI: https://doi.org/10.1109/TPWRS.2003.811178

Fang, Y., Jia, K., Yang, Z., Li, Y., & Bi, T. (2019). Impact of inverter-interfaced renewable energy generators on distance protection and an improved scheme. *IEEE Transactions on Industrial Electronics, 66*(9), 7078-7088. DOI: https://doi.org/10.1109/TIE.2018.2873521

Haddadi, A., Kocar, I., & Farantatos, E. (2019). Impact of inverter-based resources on protection schemes based on negative sequence components. *IEEE Transactions on Power Delivery, 36*(1), 289-298. DOI: https://doi.org/10.1109/TPWRD.2020.2978075

Hansen, A. D., & Michalke, G. (2007). Fault ride-through capability of DFIG wind turbines. *Renewable Energy, 32*(9), 1594-1610. DOI: https://doi.org/10.1016/j.renene.2006.10.008

Hooshyar, A., Azzouz, M. A., & El-Saadany, E. F. (2015). Distance protection of lines emanating from full-scale converter-interfaced renewable energy power plants - Part I: problem statement. *IEEE Transactions on Power Delivery, 30*(4), 1770-1780. DOI: https://doi.org/10.1109/TPWRD.2014.2369479

Hooshyar, A., El-Saadany, E. F., & Sanaye-Pasand, M. (2016). Fault type classification in microgrids including photovoltaic DGs. *IEEE Transactions on Smart Grid, 7*(5), 2218-2229. DOI: https://doi.org/10.1109/TSG.2015.2451675

Institute of Electrical and Electronics Engineers [IEEE], & North American Electric Reliability Corporation [NERC]. (2018). *Impact of inverter based generation on bulk power system dynamics and short-circuit performance*. New York: NY: IEEE.

Jia, K., Yang, Z., Fang, Y., Bi, T., & Sumner, M. (2019). Influence of inverter-interfaced renewable energy generators on directional relay and an improved scheme. *IEEE Transactions on Power Electronics, 34*(12), 11843-11855. DOI: https://doi.org/10.1109/TPEL.2019.2904715

Kauffmann, T., Karaagac, U., Kocar, I., Jensen, S., Farantatos, E., Haddadi, A., & Mahseredjian, J. (2019). Short-circuit model for type-IV wind turbine generators with decoupled sequence control. *IEEE Transactions on Power Delivery, 34*(5), 1998-2007. DOI: https://doi.org/10.1109/TPWRD.2019.2908686

Lee, J., & Zhao, F. (2021). *Global wind report 2021*. Brussels, BE: GWEC.

Morren, J., & Haan, S. W. H. (2007). Short-circuit current of wind turbines with doubly fed induction generator. *IEEE Transactions on Energy Conversion, 22*(1), 174-180. DOI: https://doi.org/10.1109/TEC.2006.889615

Piya, P., Ebrahimi, M., Karimi-Ghartemani, M., & Khajehoddin, S. A. (2018). Fault ride-through capability of voltage-controlled inverters. *IEEE Transactions on Industrial Electronics, 65*(10), 7933-7943. DOI: https://doi.org/10.1109/TIE.2018.2803765

Singh, M., & Santoso, S. (2011). *Dynamic models for wind turbines and wind power plants*. Austin, TX: NREL.

Wu, Y. K., Lin, Z.-T., Lee, T.-C., Hsieh, T.-Y., & Lin, W.-M. (2016). Adaptive setting and simulation of distance protection relay in a long transmission system connected to an offshore wind farm. *Journal of Clean Energy Technologies, 4*(6), 401-407. DOI: https://doi.org/10.18178/JOCET.2016.4.6.321